Validation of an Aero-Acoustic Wind Turbine Noise Model Using Advanced Noise Source Measurements of a 500kW Turbine

Franck Bertagnolio, Helge Madsen, Andreas Fischer, Christian Bak

Validation of an Aero-Acoustic Wind Turbine Noise Model Using Advanced Noise Source Measurements of a 500 kW Turbine

Franck Bertagnolio[1]*, Helge Aa. Madsen[1], Andreas Fischer[1], Christian Bak[1]

ISROMAC 2016

International Symposium on Transport Phenomena and Dynamics of Rotating Machinery

Hawaii, Honolulu

April 10-15, 2016

Abstract

The measurement of a 500 kW stall-regulated wind turbine is investigated. Microphones located relatively close to the wind turbine are used to measure its acoustic emission. The operational conditions of the turbine, such as wind speed, are simultaneously monitored. In parallel, a wind turbine rotor noise model is presented. It includes the main sources of aeroacoustic noise from wind turbines: turbulent inflow, trailing edge and stall noise. The noise measured by one microphone located directly downstream of the wind turbine is compared to the model predictions at the microphone location. A good qualitative agreement is found. When wind speed increases, the rotor noise model shows that at high frequencies the stall noise becomes dominant. It also shows that turbulent inflow noise is dominant at low frequencies for all wind speeds and that trailing edge noise is dominant at low wind speeds and at frequencies above 200 Hz.

Keywords

Wind Turbine Noise — Field Measurements — Modelling — Code Validation – Turbulent Inflow Noise – Trailing Edge Noise – Stall Noise

[1] *DTU Wind Energy, Technical University of Denmark, Roskilde, Denmark*

***Corresponding author**: frba@dtu.dk

INTRODUCTION

As part of a self-financed project at DTU Wind Energy, the acoustic measurements of a wind turbine together with a series of sensors monitoring the wind turbine itself, as well as sensors on a nearby met mast (meteorology mast), have been conducted in August-October 2015. On one hand, one goal is to develop and improve existing acoustic measurement techniques for wind turbine applications, and in particular to provide a more detailed knowledge of various wind turbine noise characteristics, such as directivity, amplitude modulation, etc., which can be difficult to measure in an outdoor environment. On the other hand, the measurement campaigns conducted within this project will be used as a test bench for validating existing engineering modelling tools for wind turbine noise. This paper concentrates on the latter part of the project.

Back in 2008, a 2 MW wind turbine was equipped with multiple sensors so that its operation could be closely monitored. In particular, pressure taps and pitot tubes together with a met mast gave access to a good description of the aerodynamics phenomena occuring on the blade [1, 2, 3]. As a predecessor for the present study, 50 surface pressure microphones were flush-mounted and distributed around an airfoil profile section located on the outer radius of the blade. These microphones can measure from approximately 100 Hz up to 50 kHz and are therefore well suited for aeroacoustic phenomena. Though not directly measuring acoustic noise but pseudo-sound instead (i.e. the hydrodynamic pressure fluctuations in the blade section boundary layer), the measurements could be used to partly validate existing models for turbulent inflow noise (Amiet's model) and trailing edge noise (TNO model) in the context of a real wind turbine [4].

In the present set-up, a smaller 500 kW wind turbine is studied. The idea is to develop a new technique for the surface pressure microphones. This time, these will be glued on the airfoil blade near the leading and trailing edges. In total, 6 microphones of this type will be used. In addition, 8 field microphones will be located on the ground evenly spaced around the wind turbine in order to measure acoustic noise. Concerning the turbine itself, the existing SCADA (supervisory control and data acquisition) system will be used to monitor rotational speed, pitch, yaw and other critical parameters characteristic of the wind turbine operation. A pitot tube mounted on one of the blade will provide detailed measurement data of the atmospheric flow impinging both the rotor as a whole, and the blades. The nearby met mast provides more general information about the atmospheric conditions such as wind shear and direction, as well as turbulence characteristics.

At the time of writing, a first experimental campaign has been conducted for which noise was measured by 4 ground microphones located around the turbine. The wind turbine rotor and met mast parameters were monitored. Within short time, a second campaign will include the pitot

tube measurements together with the initial set up. Finally, within a month, a third campaign should include the entire set including surface pressure microphones on the blades. It is intended that the results of these campaigns will be presented at the conference. In this paper, only the available results obtained during the first campaign are presented.

On the modelling side, since several years a continuous effort toward the modelling of wind turbine aeroacoustics has been undertaken at DTU Wind Energy [5, 6, 7]. More recent studies have concentrated on engineering models for what is recognized by the wind turbine noise community as the main aeroacoustic noise sources from a wind turbine: turbulent inflow noise, trailing edge noise and stall noise. A number of models have been implemented and improved. As part of the present study, these models have been implemented as a sub-component of the in-house aeroelastic code HAWC2 [8, 9] which is extensively used as a tool for wind turbine design and structural load predictions, both for research purposes but also in the wind energy industry such as by wind turbine manufacturers or wind farm operators. This results in a stand-alone software that is able to simulate wind turbine rotor noise.

This paper is organized as follows. The experimental set-up is described in the next section, and the modelling tool in Section 2. In Section 3, the model results and experimental data are compared and analyzed. A discussion on these results and perspectives conclude the paper.

Table 1. NTK 500 Specifications

Rotor	
Rotor diameter	41.1 m
Swept area	1320 m^2
Rotational speed	27.1 rpm
Tilt	2^o
Coning	0^o
Blades	
Blade type	LM 19.1
Blade profiles	NACA-63-4xx* & FFA-W3-xxx*
Blade length	19.04 m
Blade chord	0.265 - 1.63 m
Blade twist	0.02 - 20.0^o
Air brakes	Pivotal blade tips
Drive train	
Power regulation	Passive aerodynamic stall
Gearbox	Flender, ratio 1:55:35
Generator	Siemens 500 kW, 4 poles, 690 V
Tower	
Type	Conical steel tube, height=33.8 m
Hub height	36 m

* 'xx' and 'xxx' denote the varying airfoil thicknesses along the span

1. EXPERIMENTAL SET-UP

The test wind turbine, which is located at DTU - Risø Campus (Roskilde, Denmark) is a traditional three-bladed stall-regulated Nordtank, NTK 500/41 wind turbine (see picture in Fig. 1 and main specifications in Table 1). The turbine is primarily used for energy production and tests.

Figure 1. Nordtank 500/41 Turbine at Risø Campus

Presently, the experimental facility is instrumented as described in the following. A 36 m met mast is placed 2 1/2 rotor diameters in the westerly direction from the wind turbine. The mast is equipped for measurement of wind speed at various heights, wind direction, air temperature, air barometric pressure and air humidity.

Various sensors are installed to measure the operational conditions of the wind turbine. The position of the nacelle (yaw), the wind direction and the wind speed on top of the nacelle are measured. Pulses from sensors placed on the fast rotating generator shaft and on the slow rotating main shaft are used to determine the rotational speeds. Status information on tip position, grid connection and shaft brake are registered. Finally, the electric power production is derived by integrating measurements of the 690 V line voltages and currents in the time domain using the Time Division Multiplication Principle.

A PC-based data acquisition system has been designed to monitor and collect data from the wind turbine and met mast sensors. The output signals from all sensors are conditioned to a ±5 V range. Analogue signals are either continuously varying (e.g. temperature), digital types such as train of pulses (e.g. rotational speed, anemometer) or on/off levels (status signals for brake, blade tips and generator modes). All signals are connected to one of three data acquisition units (DAU), each of which provides 16 analogue input channels and 6 general-purpose digital input channels. The analogue inputs are converted into 16-bit quantities. The sampling rate at the DAUs is set to 35 Hz.

Microphones manufactured by BSWA Technology Co. (ref. MPA 261 combining a 1/2″ microphone and a preamplifier) are placed around the wind turbine at a distance

of 45 m from the tower. These microphones have a nearly flat frequency response within a range varying from 20 Hz to approximately 10 kHz. The microphone signals are recorded with a National Instruments PXI acquisition platform sampling at 51.2 kHz. The microphones are placed under half-spherical wind shields which are both taped onto a 1 m diameter circular varnished plywood board. The boards are lying on the ground at specific locations around the turbine (see Fig. 2).

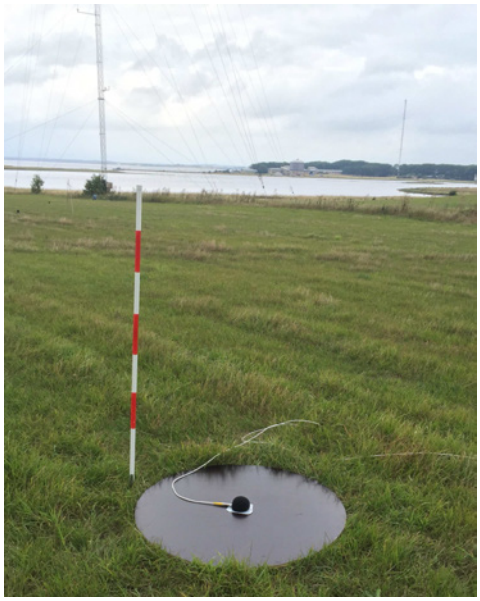

Figure 2. Microphone covered by wind shield on plywood board (Met mast on the upper left of the picture)

Finally, the overall acquisition system is designed so that all measurement devices are synchronized in time.

2. ROTOR NOISE MODEL

Wind turbine aeroacoustic noise is dominated by three main mechanisms: inflow turbulence noise, trailing edge noise and stall noise. A number of engineering models have been implemented and improved at DTU Wind Energy in order to predict these noise sources. Note that tip noise is not recognized as a problem by wind turbine manufacturers [10]. The models apply to any given airfoil section of finite span. In this section, the indices 1, 2, 3 (alternatively x, y, z) denote the streamwise direction, the normal to the airfoil plane and the spanwise direction, respectively.

2.1 Turbulent Inflow Noise

The turbulent inflow noise is modelled using Amiet's theory [11]. The radiated far-field noise spectrum generated by the surface pressure fluctuations originating from the atmospheric turbulence in our case is given as:

$$S(\boldsymbol{r},\omega) = \left(\frac{\omega\,\rho_0\,b\,y}{c_0\,\sigma^2}\right)^2 \pi U d\,|L(\boldsymbol{r},K_1,K_3)|^2\,\Phi_{22}(K_1,K_3)$$

where $\boldsymbol{r}=\{x,y,z\}^T$ is the observer location relatively to the airfoil center, b and d are the airfoil half-chord and half-span, $K_1=\omega/U$ is the convective wave-number, $K_3=\omega\,z/c_0\,\sigma$, Φ_{22} is the spectrum of the turbulence inflow component normal to the airfoil integrated along the normal wave-number k_2, $\sigma^2=x^2+\beta^2(y^2+z^2)$ and $\beta^2=1-M^2$. The Mach number is defined as: $M=U/c_0$, where c_0 is the sound velocity. The effective lift response is calculated from the response function g as:

$$L(\boldsymbol{r},K_1,k_3) = \int_{-1}^{1} g(\xi,K_1,k_3)\,\mathrm{e}^{-i\mu\xi(M-x/\sigma)}\,\mathrm{d}\xi$$

where $\mu=MK_1b/\beta^2$ and g is the airfoil response function to a vertical gust (see its detailed derivation in [12]). The turbulence impacting a wind turbine mainly originates from the atmospheric boundary layer, but may be reinforced by the wake of one or several upstream turbines. The above model in its original form uses the isotropic von Kármán spectrum to describe the turbulent inflow. However, it is well known that atmospheric turbulence is not isotropic and the model has been modified to include anisotropy using the so-called Mann model [13]. In practice, this model gives access to six independent components of the spectral tensor in a coordinate system related to the atmospheric boundary layer. Here, this tensor is rotated into the airfoil section coordinate system and the diagonal term corresponding to the normal to the airfoil plane Φ_{22} is extracted as required in the above formula.

2.2 Trailing Edge Noise

Concurrently with inflow noise, the trailing edge noise is recognized as the second dominant noise source for wind turbines. Several studies have been conducted at DTU Wind Energy [14, 15] to improve the so-called TNO model [16] which original version suffers from deficiencies, in particular for high angles of attack. The model takes the following form:

$$\Phi_p(\boldsymbol{k}_{\|},\omega) = 4\,\rho_0^2\,\frac{k_1^2}{k_1^2+k_3^2}\int_0^{\delta_{\mathrm{BL}}} 2\,L_2(y)\left(\frac{\partial U_1}{\partial y}(y)\right)^2 \times \overline{u_2^2}(y)\,\widetilde{\Phi}_{22}(\boldsymbol{k}_{\|},\Lambda)\,\Phi_m(\omega-U_c(y)k_1)\,\mathrm{e}^{-2k_{\|}y}\,\mathrm{d}y$$

where δ_{BL} is the BL thickness, L_2 is the vertical correlation length characterizing the vertical extent of the vertical turbulent velocity component u_2, $\overline{u_2^2}$ its mean squared value, U_1 is the streamwise mean velocity, $k_{\|}$ is the norm of the wavenumber vector $\boldsymbol{k}_{\|}=(k_1,k_3)$ spanning the plane parallel to the wall, $\widetilde{\Phi}_{22}$ is the normalized spectrum of the vertical velocity fluctuations integrated over k_2, Φ_m is the so-called moving axis spectrum which describes how $\widetilde{\Phi}_{22}$ is distorted by the generation and destruction of eddies during their convection past the TE. It is here approximated as a Dirac delta function assuming frozen turbulence. The convection velocity U_c of these eddies is related to the local velocity as: $U_c(y)=0.7\,U_1(y)$. Note that $\widetilde{\Phi}_{22}$ depends on the integral

length scale Λ (see definition below) and is therefore also a function of y.

Using the classical von Kármán model and introducing anisotropy stretching factors [17], the vertical velocity spectral tensor $\widetilde{\Phi}_{22}$ reads:

$$\widetilde{\Phi}_{22}(\boldsymbol{k}_{\|}, \Lambda) = \frac{4}{9\pi}\,\Lambda^2\,\beta_1\beta_3\,\frac{(\beta_1\Lambda k_1)^2 + (\beta_3\Lambda k_3)^2}{[1 + (\beta_1\Lambda k_1)^2 + (\beta_3\Lambda k_3)^2]^{7/3}}$$

where the integral length scale Λ characterizes the size of the energy-containing eddies, the coefficients β_1 and β_3 are anisotropic stretching factors in the streamwise and spanwise directions, respectively. Following the approach by Lynch *et al* [18] and introducing the stretching factors in the derivation, the correlation length L_2 is defined as a frequency dependent quantity:

$$L_2(\omega) = \frac{55\,\Gamma(1/3)}{108\,\sqrt{\pi}\,\Gamma(17/6)}\Lambda\,\beta_2\,\frac{3 + 11(\beta_1\Lambda k_c)^2}{3 + 8(\beta_1\Lambda k_c)^2} \times \frac{1}{\sqrt{1 + (\beta_1\Lambda k_c)^2}}$$

where $k_c = \omega/U_c$ is the convective wavenumber and β_2 is an additional anisotropy stretching factor in the direction perpendicular to the airfoil surface. The integral length scale is deduced from the Prandtl mixing length l_m as:

$$\Lambda = l_m/(0.747\kappa)$$

where $\kappa = 0.41$ is the von Kármaán constant and l_m is given across the boundary layer as:

$$l_m = 0.085\,\delta_{\text{BL}}\tanh(\kappa y/(0.085\,\delta_{\text{BL}}))$$

The turbulent stress $\overline{u_2^2}$ is approximated as $0.45\,k_T$ and $0.3\,k_T$ on the airfoil suction and pressure sides, respectively, and the turbulent kinetic energy k_T across the boundary layer is evaluated as:

$$k_T = \sqrt{\left(\nu_t\frac{\partial U_1(y)}{\partial y}\right)/C_\mu}$$

where $\nu_t = l_m^2|\partial U_1(y)/\partial y|$.

In order to close the model and as a result of a tuning procedure using experimental data (see [15] for details), the anisotropy stretching factors are given as:

$$\beta_1 = 0.4 \quad \text{and} \quad \beta_2 = (\gamma)^{1/5} \quad \text{and} \quad \beta_3 = (2\,\gamma)^{1/2}$$

using the following non-dimensional BL pressure gradient along the airfoil chord defined as:

$$\gamma = \frac{\delta_{\text{BL}}}{U_\tau}\left[\frac{(\partial P/\partial x_1)^2}{\rho_0\,\mu}\right]^{1/3}$$

where P is the mean static pressure, U_τ is the friction velocity, and μ the dynamic viscosity.

The far-field noise spectrum $S(\omega)$ can be deduced from the SP spectrum model defined above using Howe's theory [19]. For an observer located at a distance R above the TE orthogonally to the flow leaving the TE and in the limit of low Mach number flow, it reduces to [20]:

$$S(\omega) = \frac{L}{4\pi R^2}\int_{-\infty}^{+\infty}\frac{\omega}{c_0|k_1|}\,\Phi_p(\omega, k_{\|})|_{k_3=0}\,\mathrm{d}k_1$$

where L is the span of the considered airfoil section.

2.3 Stall Noise

Finally, there exist evidences that stall noise can under certain conditions produce Amplitude Modulation noise [21] and is certainly a major noise source in the case of stall-regulated wind turbines. Recently, a stall noise model has been developped at DTU Wind Energy [22] and although this model has been partially validated against wind tunnel measurements, the present experiment is a good opportunity to test the model in real conditions since the tested wind turbine is a stall-regulated one.

The far-field stall noise spectrum is adapted from Amiet's formulation as in Section 2.1 but in its adapted version for trailing edge noise [23] and as a function of the frequency surface pressure spectrum as:

$$S(\omega, \boldsymbol{x}) = \left(\frac{\omega\,x_2}{4\pi c_0 S_0^2}\right)^2 2\pi L\,|G(K_c, K_1, K_3)|^2 \times S_{pp,te}(\omega)\,\Gamma_{3,te}(\omega, K_3)$$

where the subscript $_{,te}$ denotes a quantity evaluated at the TE. S_{pp} is the surface pressure spectrum, whereas Γ_3 is the normalized cross-correlation spectrum in the span direction. The function G is the equivalent of the lift function introduced in Amiet's model. It reads:

$$G(K_c, K_1, K_3) = \int_0^C g(y_1, K_c, K_1, K_3)\,\mathrm{d}y_1$$

and includes both the incident and scattered field contributions. It is here evaluated numerically instead of analytically as in Amiet's derivation [23].

It is noteworthy that the three models described above are all based on the knowledge of the surface pressure spectra which will be measured at a later stage during this project (see Introduction).

2.4 Noise Models Implementation

In order to model and analyze wind turbine noise, the above models have been implemented within the in-house aeroelastic code HAWC2 [8, 9] used for time-domain simulations of wind turbines. This code uses the Blade Element Momentum theory as a basis for the modelisation of the aerodynamic flow around the rotor. The structure is modelled using a multi-body formulation.

Using the same discretization as for the blade elements in the HAWC2 code, the noise from the three models presented in the previous section is calculated for each blade

element (assuming a constant chord and thickness of the airfoil section along the span extent of each element) at a specified observer location and the results are integrated across the whole blade span and for the three (or the actual number of) blades of the turbine. Thus, together with the atmospheric and geometric input data from the measurement campaign, the combined aeroelastic and aeroacoustic simulation tool is able to reproduce the noise generation mechanisms at an observer located near the wind turbine. Indeed, no propagation effects (such as atmospheric effects or ground reflection, diffraction by obstacle) are included in the present model, except for distance from source to observer and directivity. Therefore, the noise predictions are only expected to be reliable within a couple of 100 m from the turbine. The directivity is implicitly included in the turbulent inflow and stall noise model formulations. As for the trailing edge noise model, the functions proposed by Brooks *et al* [24] discriminating between low and high frequencies are used:

$$D_l = \sin^2(\theta)\sin^2(\phi) \quad \text{and} \quad D_h = 2\sin^2(\theta/2)\sin^2(\phi)$$

where θ is the angle between the plane formed by the trailing edge and the normal to the airfoil plane and the one formed by the trailing edge and the observer location, whereas ϕ is the angle measuring the elevation of the observer relatively to the airfoil plane. A convective amplification correction is applied to all models, again at low and high frequencies:

$$C_l = 1/(1+M_r\cos\theta_c)^4 \quad \text{and} \quad C_h = 1/(1+M_r\cos\theta_c)^3$$

where M_r is the Mach number of the airfoil velocity relatively to the observer and θ_c the angle between this relative velocity and the airfoil-observer direction. The threshold between the low and high frequencies is conditioned by the airfoil being acoustically compact or not. Doppler shift effects are also accounted for in the models.

Concerning the input data for the HAWC2 code, the authors have access to all the data relative to the geometry of the wind turbine since it is owned by DTU Wind Energy. The atmospheric inflow conditions are determined from the data collected on the met mast or by the anemometer on the nacelle. As for the blade aerodynamic properties required for the Blade Element Momentum method, the input data consist of the aerodynamic lift, drag and moment coefficients as a function of the angle of attack for each specific airfoil shapes along the blade. These are provided as look-up tables that have been corrected for 3D effects [25] and validated in earlier studies.

Independently from the above aerodynamic data used for the rotor aerodynamic, the noise models necessitate the knowledge of more detailed aerodynamics around the airfoil sections. This amounts to: 1) the relative flow velocity impinging each airfoil section along the blade 2) the atmospheric turbulence characteristics impacting each airfoil section for the turbulent inflow noise 3) the boundary layer properties near the trailing edge for the trailing edge noise 4) the separation location for the stall noise model. These data are partly available from the aeroelastic code itself. The atmospheric turbulence characteristic quantities are prescribed by the user. The remaining information are generated in a pre-processing step using the airfoil flow analysis code Xfoil [26] and stored as look-up tables. Xfoil is a 2D flow solver that requires as input the airfoil genometry, the relative inflow velocity and angle of attack. These are readily available from the aeroelastic code. The boundary layer profile is calculated using Coles law of the wall/wake [27]. As a consequence of the 2D assumption, the impact of the 3D inflow on the noise generation is neglected here, though it is believed to be negligeable in particular in the outer part of the blades where the flow should be more two-dimensional and where most of the aeroacoustic noise is produced. The separation location is also provided by the Xfoil code and the accuracy of this calculation may be questionable, in particular at high angles of attack but this is so far the easiest evaluation method.

As a result, the above simulation framework is a stand-alone software tool that is able to simulate wind turbine rotor noise in the time-frequency domain. It should be reminded here that the noise models provide results as sound power spectra. Typically, the aeroelastic code uses time-steps of the order of 0.01 s. Therefore, in principle the combined aero-elastic/acoustic model is able to simulate sound down to 100 Hz, though it is safe to consider quite lower frequencies assuming that no phenomenon significant for the wind turbine aeroelastic behavior occurs at these frequencies. Nevertheless, concerning turbulent inflow noise and for sufficiently large inflow vortices (i.e. low wavenumbers) blade-to-blade correlation effects arise and concentrate sound energy around blade passage harmonics. Given the design turbine rotational speed of 27.1 rpm and the size of the blades, one can expect that these effects fades away above approximately 2.2 Hz which is much lower than the frequencies of interest here. Consequently, this phenomenon is not included in the present model.

Note that the aeroelastic code includes atmospheric turbulence for determining the inflow impacting the wind turbine rotor. Therefore, the simulations are unsteady and the inflow conditions onto each blade section used as an input for the three noise models are varying in time (on top of the periodic variations resulting from the atmospheric shear and the rotating blades). As for the model results displayed in the next section, the calculated noise is averaged in time over one rotor revolution (approximately 2.2 s). This might not ensure convergence of the results since the characteristic time of atmospheric turbulence is longer, but the computational cost of the noise models prevented to perform much longer simulations during the present study. This averaging period for the noise model calculations is performed when the wind turbine aeroelastic dynamic has reached a statistical steady-state.

3. ANALYSIS OF RESULTS

3.1 Experimental Data Post-Processing

In this paper, only the measurement data recorded by the microphone located directly downwind of the wind turbine at a distance of 45 m from the tower are considered.

The time-series recorded by the microphone are splitted into 2.2 s sub-series (corresponding to approximately one rotor rotation period). These sub-series are then binned according to the wind speed measured simultaneously by the nacelle cup anemometer, i.e. the wind speed averaged during the corresponding 2.2 s time periods. A velocity penalty of 0.5 m/s is applied to the measured nacelle wind speed to account for the inflow deceleration caused by the rotor induction. The binned time-series are Fourier transformed and the Sound Pressure Levels in $^1/_3$ octave bands are reduced by 6 dB to account for the doubling of the pressure due to the ground plates. Note that the sub-series are further sub-divided in shorter time-series, applied a Hanning window and the resulting spectra are averaged. This averaging process includes all the sub-series contained in each individual bin as introduced above.

3.2 Background Noise

As a first part of the analysis, the background noise in the measurements data is evaluated. Similar data post-processing as described in the previous section is applied to the microphone recordings, though without velocity penalty, when the wind turbine is shut down. The sound spectra are plotted at two averaged wind speeds $U = 9$ and 13 m/s in Fig. 3. It is clear that there exists a significant increase of the power spectral energy over the whole spectral range when the turbine is operating. A peak clearly emerges at 1 kHz when the turbine is operating. It is attributed to mechanical noise from the gearbox. Between 200 and 400 Hz, a broadband hump is clearly visible both in the background noise and when the turbine is operating. Furthermore, it seems that background noise is also important from 800 to 2000 Hz. The former hump may originate from car traffic on a moderately busy road located approximately 150 m away from the turbine. The latter noise increase is probably caused by vegetation noise that was quite predominant the day the measurements took place. Indeed, the wind turbine is located among crop fields and the measurements were performed a couple of weeks before harvest. However, it is difficult to attribute specific measured background noise to specific sources. Nevertheless, it is also observed that the signal to noise ratio increases significantly as the wind speed increases.

In the above plots, the sound spectra recorded when the turbine is operating are corrected by simply substracting the background noise spectra. As expected, it has little effect of the spectrum measured at the highest wind speed, but it has a significant impact at $U = 9$ m/s in the frequency range 700 to 2500 Hz. On both sides of the peak centered at 1 kHz, the corrected spectrum even becomes lower than the background noise. Therefore, the results of this type of background noise correction must be interpreted with caution.

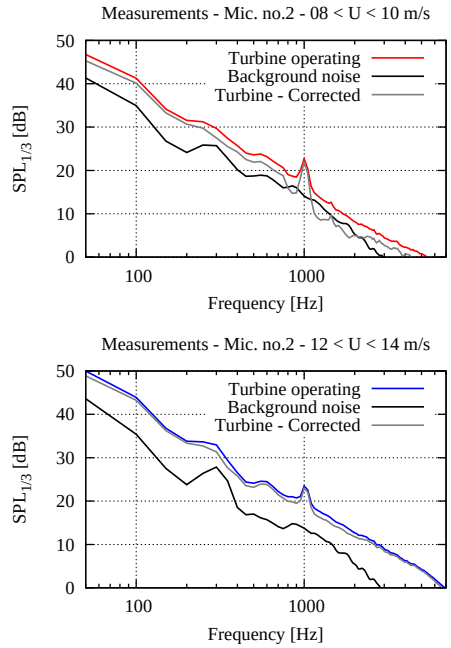

Figure 3. Wind turbine noise compared to background noise

3.3 Model versus Measurement Data

The wind turbine noise at various wind speeds is analyzed next. In Fig. 4, the acoustic noise measured by the microphone located downwind of the wind turbine (referred to as mic. no. 2) is qualitately compared with predictions from the wind turbine noise model at the same location, including all three noise sources described in Section 2. The model calculations are performed during 2.2 s in real time (i.e. one rotor revolution) and the results are averaged over this time period. Note that for the model results presented in this section, the turbulent inflow noise model makes use of the von Kármán spectrum. As an input for this spectrum definition, the turbulence intensity is estimated from wind speed recordings on the met mast and is set equal to 10%. The turbulence integral length scale is set to 0.7 times the distance from the ground up to 60 m height where it becomes constant, as suggested in the IEC 64000-1 standard for wind turbine loading studies.

Two mean wind speeds are considered: $U = 9$ and 13 m/s. As it can be seen, there exists a quite good agreement between the model and experiment, though the model under-estimates the measurements at frequencies below 100 Hz and slightly over-estimates them between 100 and 1 kHz.

In these plots, the measured spectra corrected for background noise are also displayed. At $U = 9$ m/s, the over-prediction by the model becomes even more severe for these corrected data, in particular between 700 and 2500 Hz. But, as mentioned in Section 3.2 this correction should be

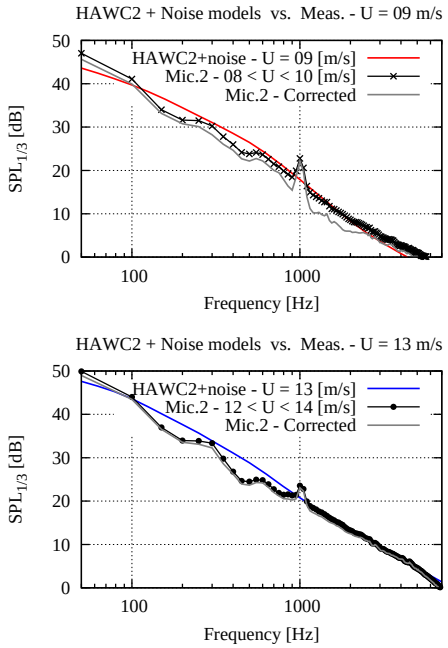

Figure 4. Wind turbine noise compared to HAWC2 rotor noise model

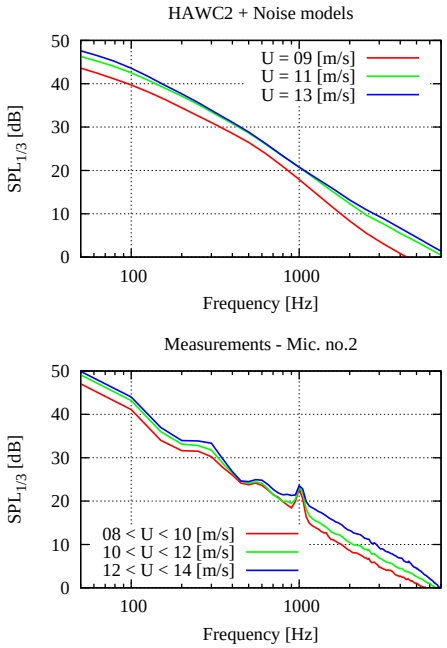

Figure 5. Wind turbine noise at various wind speeds

cautiously interpreted.

The influence of the wind speed is investigated separately for the measurements and the model in Fig. 5. Three mean wind speeds are considered: $U = 9$, 11 and 13 m/s. Both model and experimental results predict a similar increase in spectral energy across the whole frequency range. At the highest velocity $U = 13$ m/s this energy increase is more significant at frequencies above 1 kHz. As it will be shown below, this is consistent with the stall-regulation of the turbine power when it reaches its maximum at higher wind speeds.

3.4 Noise Mechanisms Identification

In this section, the respective contributions of the different noise sources are investigated. The numerical model readily gives access to the different noise sources since these can be stored individually in the course of the time-domain simulations.

Fig. 6 display the different noise source contributions at $U = 9$ and 13 m/s. It is clear that at low frequencies, turbulent inflow noise is dominant. Therefore, further investigations for improving the discrepancies observed in the previous section at low frequencies should be targeted at this model (see Section 3.5). At high frequencies (above 1 kHz), the figure clearly shows that stall noise becomes dominant. This is in good agreement with experimental data as observed in the previous section when stall-regulation kicks in at high wind speeds.

3.5 Effect of Inflow Turbulence Model

As mentioned earlier, the classical turbulent inflow noise proposed by Amiet [11] makes use of the von Kármán spectrum to characterize the inflow turbulence impinging the airfoil. The effect of using Mann model [13] for atmospheric turbulence is investigated here. As input for Mann model, a standard value for neutral atmospheric conditions is assumed for the anisotropy parameter $\Gamma = 3.7$ which somehow is a measure of the wind shear and is assumed constant across the rotor plane. The turbulence length scale is defined in the same way as for the von Kármán model in Section 3.3. Finally, the model requires a measure of the energy dissipation rate $\alpha\epsilon^{2/3}$ (here α is an empirical constant and ϵ is the turbulent kinetic energy dissipation rate) which ultimately defines the spectral energy level. This is achieved by defining a characteristic roughness length z_0 for the terrain in the turbine area. It is used to define the friction velocity $u_* = \kappa U_H / \log(H/z_0)$ such that the hub velocity U_H matches a logarithmic profile at hub height H. Finally, the required coefficient is defined as $\alpha\epsilon^{2/3} = 2.8 \cdot u_*^2/h^{2/3}$ [28] where h is the height at which the spectrum is calculated.

In Fig. 7, the model results, using Mann's spectrum for the turbulent inflow noise model, are compared with the measurements at two wind speeds $U = 9$ and 13 m/s and for two roughness lengths $z_0 = 0.1$ and 0.5 m. As it can be seen, the model results with the latter roughness length improve the qualitative agreement with the measured spectra at low frequencies compared to the von Kármán model results. However, this roughness length is probably overestimated considering the crop field-type landscape surrounding the wind turbine (though some higher structures - trees and one building - are located at a distance of approximately 500 m in

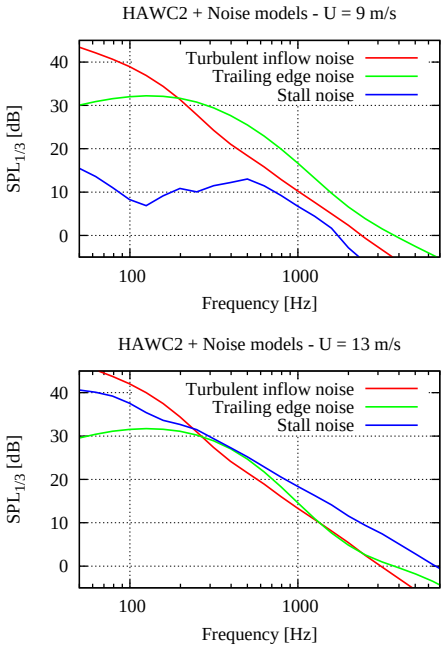

Figure 6. Wind turbine noise different source contributions

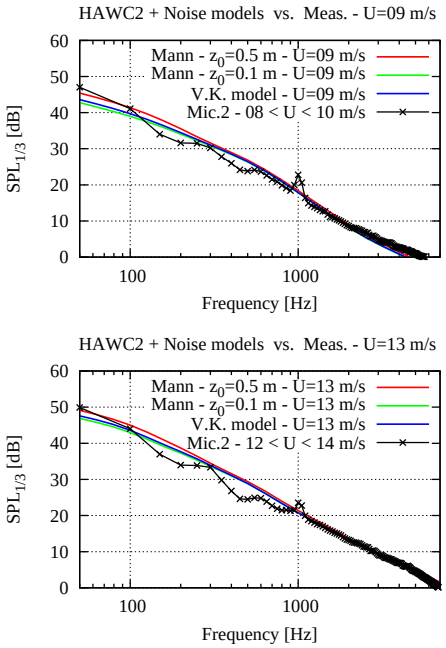

Figure 7. Wind turbine noise vs. HAWC2 rotor noise model using Von Kármán or Mann model

the general upstream direction). The value $z_0 = 0.1$ m seems a more reasonable value but exhibits even lower results than the von Kármán model.

Nonetheless, this relatively good qualitative agreement of the results may be accidental. Indeed, as explained above a standard value for neutral atmospheric conditions is assumed here. Since the measurement campaign took place on a windy and sunny day, unstable atmospheric conditions would probably be more realistic.

To conlude this section, a thorough study should be conducted in order to properly tune the input parameters for Mann model.

4. DISCUSSION AND FUTURE WORK

In this paper, a model for predicting wind turbine noise is presented. It combines a standard wind turbine aeroelastic code to various aeroacoustic noise models. The results of this combined model are compared to field measurements of a 500 kW wind turbine.

The preliminary results of this investigation show quite good quantitative agreement between the model calculations and the experimental data. Furthermore, the modelling approach enables to identify the relative importance of the various noise sources depending on wind speed which is so far consistent with measurements. It appears that trailing edge noise is dominant at low wind speeds and above 200 Hz, but that it is dominated by stall noise at higher wind speeds (for this stall-regulated turbine). At low frequencies, turbulent inflow noise dominates but it is slightly underestimated by the classical Amiet's theory using a von Kármán turbulence spectrum model. Using Mann model improves the results if a sufficiently large roughness length is used.

In the future, the experimental set-up will be extended with more field microphones located on the ground around the wind turbines. More importantly, the measurements will include a pitot tube mounted on one of the blades to monitor the local inflow velocity on the rotor. Finally, surface pressure microphones glued on the airfoil surface will be used to closely monitor the different aeroacoustic noise sources and it should in principle be possible to correlate these data with the acoustic noise measurements on the ground [29].

ACKNOWLEDGMENTS

The authors would like to thanks the people at DTU Wind Energy (TEM section) for their help in designing and conducting the field measurements: Karen Enevoldsen, Claus B.M. Pedersen, Per Hansen and Uwe S. Paulsen.

The authors are also grateful to Bo Søndergaard from Grontmij A/S for his help in setting-up the acoustic microphone measurement system and his comments regarding this work.

REFERENCES

[1] C. Bak, H. Aa. Madsen, U. S. Paulsen, M. Gaunaa, P. Fuglsang, J. Romblad, N. A. Olesen, P. Enevoldsen, J. Laursen, and L. Jensen. DAN-AERO MW: Details Aerodynamic Measurements on a Full-Scale MW Wind Turbine. In *2010 European Wind Energy Conference - EWEC2010*, Conf. Proceedings, Warsaw (Poland), March 2010.

[2] H. Aa. Madsen, C. Bak, U. S. Paulsen, M. Gaunaa, P. Fuglsang, J. Romblad, N. A. Olesen, P. Enevoldsen, J. Laursen, and L. Jensen. The DAN-AERO MW Experiments. In 48^{th} *AIAA Aerospace Sciences Meeting Including The New Horizons Forum and Aerospace Exposition*, Conference Proceedings, Orlando (FL), January 2010.

[3] H. Aa. Madsen, C. Bak, U. S. Paulsen, M. Gaunaa, P. Fuglsang, J. Romblad, N. A. Olesen, P. Enevoldsen, J. Laursen, and L. Jensen. The DAN-AERO MW Experiments - Final report. Tech. Rep. Risø-R-1726(EN), Risø-DTU, Roskilde, Denmark, September 2010.

[4] F. Bertagnolio, H. Aa. Madsen, C. Bak, N. Troldborg, and A. Fischer. Aerodynamic Noise Characterization of a Full-Scale Wind Turbine through High-Frequency Surface Pressure Measurements. *International Journal of Aeroacoustics*, 14(5-6):729–766, 2015.

[5] H. Aa. Madsen and P. Fuglsang. Numerical Investigation of Different Tip Shapes for Wind Turbine Blades - Aerodynamic and Aeroacoustic Aspects. Tech. Rep. Risø-R-891(EN), Risø Natl. Lab., Roskilde, Denmark, December 1996.

[6] H. Aa. Madsen. Low Frequency Noise from MW Wind Turbines - Mechanisms of Generation and its Modeling. Tech. Rep. Risø-R-1637(EN), Risø-DTU, Roskilde, Denmark, April 2008.

[7] W. J. Zhu, N. Heilskov, W. Z. Shen, and J. N. Sørensen. Modeling of Aerodynamically Generated Noise From Wind Turbines. *Journal of Solar Energy Engineering*, 127(4):517–528, 2005.

[8] T. J. Larsen and A. M. Hansen. How 2 HAWC2, The User's Manual. Tech. Rep. RISØ-R-1597(ver.3-1), Risø-DTU, Roskilde, Denmark, December 2007.

[9] HAWC2 Aeroelastic Simulation of Wind Turbines. `http://www.hawc2.dk`. Accessed: 2015-09-01.

[10] S. Oerlemans, P. Sijtsma, and B. Méndez López. Location and Quantification of Noise on a Wind Turbine. *J. Sound Vib.*, 299(5-6):869–883, 2007.

[11] R. K. Amiet. Acoustic Radiation from an Airfoil in a Turbulent Stream. *J. Sound Vib.*, 41(22):407–420, 1975.

[12] R. W. Paterson and R. K. Amiet. Acoustic Radiation and Surface Pressure Characteristics of an Airfoil Due to Incident Turbulence. In 3^{rd} *AIAA Aero-Acoustics Conference*, Conf. Proceedings, Palo Alto, CA, July 1976.

[13] J. Mann. The Spatial Structure of Neutral Atmospheric Surface-layer Turbulence. *Journal of Fluid Mechanics*, 273:141–168, 1994.

[14] A. Fischer. Experimental Characterization of Airfoil Boundary Layers for Improvement of Aeroacoustic and Aerodynamic Modeling. PhD Thesis, DTU, Wind Energy Department, Roskilde, Denmark, Nov. 2011.

[15] F. Bertagnolio, A. Fischer, and W. J. Zhu. Tuning of Turbulent Boundary Layer Anisotropy for Improved Surface Pressure and Trailing-Edge Noise Modeling. *Journal of Sound and Vibration*, 333:991–1010, 2014.

[16] R. Parchen. Progress report DRAW: A Prediction Scheme for Trailing-Edge Noise Based on Detailed Boundary-Layer Characteristics. TNO Rept. HAG-RPT-980023, TNO Institute of Applied Physics, The Netherlands, 1998.

[17] R. L. Panton and J. H. Linebarger. Wall Pressure Spectra Calculations for Equilibrium Boundary Layers. *J. Fluid Mech.*, 65(2):261–287, 1974.

[18] D. A. Lynch, W. K. Blake, and T. J. Mueller. Turbulence Correlation Length-Scale Relationships for the Prediction of Aeroacoustics Response. *AIAA Journal*, 43(6):1187–1197, 2005.

[19] M. S. Howe. A Review of the Theory of Trailing Edge Noise. *J. Sound Vib.*, 61(3):437–465, 1978.

[20] T. F. Brooks and T. H. Hodgson. Trailing Edge Noise Prediction from Measured Surface Pressures. *J. Sound Vib.*, 78(1):69–117, 1981.

[21] H. Aa. Madsen, F. Bertagnolio, A. Andreas, and C. Bak. Correlation of Amplitude Modulation to Inflow Characteristics. In *Internoise 2014*, Conference Proceedings, Melbourne, Australia, November 16-19 2014.

[22] F. Bertagnolio. Experimental Investigation of Stall Noise Toward its Modelling. In *6th International Conference on Wind Turbine Noise*, Conference Proceedings, Glasgow, UK, April 2015.

[23] R. K. Amiet. Effect of the Incident Surface Pressure Field on Noise Due to Turbulent Flow Past a Trailing Edge. *J. Sound Vib.*, 57(2):305–306, 1978.

[24] T. F. Brooks, S. D. Pope, and M. A. Marcolini. Airfoil Self-Noise and Prediction. NASA Reference Publication 1218, Langley Research Center, 1989.

[25] C. Bak, J. Johansen, and P. Andersen. Three-Dimensional Corrections of Airfoil Characteristics Based on Pressure Distributions. In *Proc. EWEC 2006*, Athens, Greece, 2006.

[26] M. Drela. *Low Reynolds Number Aerodynamics*, volume 54, chapter XFOIL: An Analysis and Design System for Low Reynolds Number Airfoils, pages 1–12. Mueller, T.J. (ed.), Lecture Notes in Engineering, Springer-Verlag, Berlin, 1989.

[27] D. Coles. The Law of the Wake in the Turbulent Boundary Layer. *J. Fluid Mech.*, 1:191–226, 1956.

[28] J. Mann. Wind Field Simulation. *Probabilistic Engineering Mechanics*, 13(4):269–282, 1998.

[29] H. Aa. Madsen, F. Bertagnolio, A. Fischer, C. Bak, and U. S. Paulsen. A Novel Full Scale Experimental Characterization of Wind Turbine Aero-acoustic Noise Sources. In *ISROMAC 2016*, Conference Proceedings, Honolulu (HI), April 2016.